Performance Investigation of High-Speed Train OFDM Systems under the Geometry-Based Channel Model

Do Viet Ha, Trinh Thi Huong, and Nguyen Thanh Hai

Abstract—The high-speed of train (HST) in combination with the high carrier frequency of HST systems leads to the severe inter carrier interference (ICI) in the HST orthogonal frequency division multiplexing (HST-OFDM) systems. To avoid the complexity in OFDM receiver design for ICI eliminations, the OFDM system parameters such as symbol duration, signal bandwidth, and the number of subcarriers should be chosen appropriately. This paper aims to propose a process of HST-OFDM system performance investigation to determine these parameters in order to enhance spectral efficiency and meet a given quality-of-service (QoS) level. The signal-to-interference-plus-noise ratio (SINR) has been used as a figure of merit to analyze the system performance instead of signal-to-noise ratio (SNR) as most of recent research studies. Firstly, using the non-stationary geometry-based stochastic HST channel model, the SINR of each subcarrier has been derived for different speeds of the train, signal bandwidths, and number of subcarriers. Consequently, the system capacity has been formulated as the sum of all the single channel capacity from each sub-carrier. The constraints on designing HST-OFDM system parameters have been thoughtfully analyzed using the obtained expressions of SINR and capacity. Finally, by analyzing the numerical results, the system parameters can be found for the design of HST-OFDM systems under different speeds of train. The proposed process can be used to provide hints to predict performance of HST communication systems before doing further high cost implementations as hardware designs.

Keywords—High-speed train systems, geometry-based channel models, OFDM systems, SINR, capacity

I. INTRODUCTION

ORTHOGONAL frequency division multiplexing (OFDM) is a good candidate for wideband high speed train (HST) systems because of its efficiency and robustness to multipath propagation. Compared with conventional OFDM-based communication systems, the HST-OFDM system suffers more challenges such as larger Doppler shift due to the high speed of trains and the high carrier frequency of HST systems [1], [2]. For the high speed of train of more than 350 km/h, the large Doppler shift that causes inter-carrier interference (ICI) destroys the orthogonality between the subcarriers and degrades the HST-OFDM system [1]. To deal with the severe ICI effect, complex algorithms

implemented in OFDM receivers have been proposed in many research studies to estimate the time and frequency selective HST channels [1], [3]–[5]. These algorithms add tremendous complexity on the design of synchronization and channel estimation units. To avoid the complexity in receiver design, there is in need to investigate the HST-OFDM system performance under the high Doppler shifts and then find the system design to limit the ICI effect.

Key HST-OFDM system parameters such as the symbol duration, the signal bandwidth, and the number of subcarriers should be chosen to combat both the time and frequency selectivity of HST wideband channels [6]. Especially, due to the high speed of train, the highly-time varying channels make HST-OFDM systems be quite different from other conventional ones [7]. Therefore, the rule of determining these parameters for conventional OFDM systems may not be applied well in HST-OFDM system. In most of research works [1], [7]–[11], these parameters have been chosen without analyzing the HST channel characteristics. To verify the performance gain of the proposed algorithms, the number of subcarrier $N = 128$ has been used in [8]–[10] to simulate the HST system for the different bandwidth of $B = 160\,\mathrm{MHz}$, $1.92\,\mathrm{MHz}$, and $1\,\mathrm{MHz}$, respectively. The authors in [1], [11] investigated the HST system with the simulation settings as $N = 512$ for the bandwidth of $B = 5\,\mathrm{MHz}$ and $100\,\mathrm{MHz}$, respectively. In [7], the system parameters $N = 1024$ and $B = 10\,\mathrm{MHz}$ has been selected to evaluate the down-link performance in HST systems for different speeds of the train in the range of $100\,\mathrm{km/h} - 400\,\mathrm{km/h}$. On the whole, these studies have not yet analyzed the HST channel properties to find out the appropriate HST system parameters for different train movement scenarios.

As mentioned above, the HST-OFDM system is strongly affected by the ICI noise, the signal-to-interference-plus-noise ratio (SINR) is thus an important quantity for the system analysis. Besides, the system capacity is also an important factor to design components in a communication system. However, there is a little research on evaluating the system performance in term of these factors. The capacity has been derived from the received signal-to-noise ratio (SNR) in recent research studies [5], [12]–[14], which means that the ICI effect has not been considered. The capacity of HST communication system was formulated by assuming that the SNR is not influenced by the variation of attenuation and path losses [13].

Therefore, the time-varying HST channel characteristics that causes the ICI effect has been neglect. The HST channel model that represents only path losses was used in [14] to compute the capacity. Other studies [12], [14], [15] investigated the capacity using the HST channel model which was assumed to be the Rice channel. The large-scale fading of this channel model represents the path loss factor and the shadow fading coefficient obeying the log normal distribution. Meanwhile, the small-scale fading channel coefficient was the independently and identically distributed (i.i.d.) Rice distribution. Thus, these studies did not analyze the channel capacity under a specific HST movement scenario with the effect of Doppler shifts. In [5], the HST channel model with the time-varying small-scale parameters that describes HST specific scenarios were use to analyze the capacity. However, the ICI effect was not considered in capacity computation because the capacity was derived from the SNR. In short, there is lack of studies that evaluate the capacity under the influence of ICI noise with the time-varying HST channel model for HST specific movement scenarios.

To investigate and test the HST-OFDM systems, there is essential to have channel models which capture accurately the multipath propagation and the time-varying characteristics due to the high speed of trains [2]. However, the modeling of the propagation channel in HST environments is still challenging [5]. The wide-sense stationary (WSS) condition was assumed to reduce the complexity in modeling the HST channels [2]. However, the measurement results of HST scenarios in [16], [17] show that the assumption is not valid. Furthermore, the non-stationary properties of the HST channel could not be neglect in the physical layer design and performance evaluation as shown in some related measurements for HST communication systems [18]. It is therefore necessary to model HST channels with the non-stationary properties. The non-stationary HST geometry-based stochastic model (GBSM) was first proposed in [19] with the time-varying distance between the transmitter (Tx) and the receiver (Rx). Some more parameters such as the angles of arrival (AoAs) and angles of departure (AoDs) were also considered as time-variant to further improve the non-stationary GBSM [20].

This paper uses the novel non-stationary wideband HST channel model proposed in [20] and further improved in [18] to evaluate the capcity performance of HST-OFDM system. Furthermore, the HST measurement results in [21] have been used to configure the channel model for the purpose of making it realistic. Using the channel simulation model, the SINR of each subcarrier in HST-OFDM system has been derived, then the capacity is formulated using the SINR results. In other words, the impact of Doppler frequency and ICI effect on the capacity performance are thoroughly investigated. By analyzing both SINR and capacity results, a set of system parameters including the signal bandwidth, the number of subcarriers, and the OFDM symbol duration has been chosen to maximum the channel capacity or to meet the SINR requirements for a given quality-of-service (QoS) level.

The remainder of this paper is organized as follows. In Section II, the wideband geometry-based HST channel model is described. The expression of SINR and capacity of the HST-OFDM system under the non-stationary HST channel model is derived in Section III. The simulation results are presented and analyzed in Section IV. Finally, the conclusions are drawn in Section V.

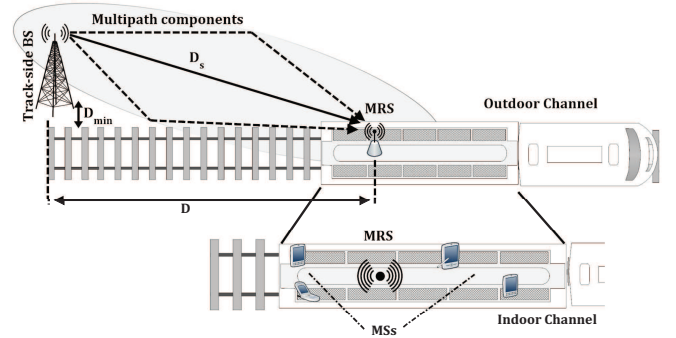## II. THE NON-STATIONARY WIDEBAND HST CHANNEL MODEL

Fig. 1. A HST communication system deploying MRSs [20]

Figure 1 illustrates the HST communication system deploying MRSs (Mobile relay station) to improve the system performance [20]. There are two types of wireless channel in the system: the outdoor channel between the BS (Base Station) and the indoor channel between MRS and MS (on-board mobile stations). This paper aims to investigate the outdoor channel.

As illustrated in Fig. 2, the wideband geometry-based HST channel model consists of I con-focal ellipses with the BS and the train at their foci, where I denotes the total number of ellipses or taps. The time-varying distance between BS and MRS is given by $D_s(t) = \sqrt{D_{\min}^2 + D^2(t)}$, where $D_{\min} = 50\,\mathrm{m}$ stands for the minimum between BS and the track; $D(t)$ denotes the projection of $D_s(t)$ on the railway track plane. There are N_i scatterers lying on ith ellipse (i.e., ith tap). Let assume $a_i(t)$ be the semi-major axis of the ith ellipse, and its time-varying semi-minor $b_i(t)$ can be computed by

$$b_i(t) = \sqrt{a_i^2(t) - f_s^2(t)}, \qquad (1)$$

where $f_s(t) = D_s(t)/2$ represents the half distance between the two foci of ellipses. The other geometrical parameters of the HST model are listed in Table I. The complex time-variant channel impulse response (TVCIR) of the link between BS and MRS can be given by $h(t, \tau) = \sum_{i=1}^{I} h_i(t)\delta(\tau - \tau_i)$, where $h_i(t)$ and τ_i are the complex channel gain and the propagation delay of ith the tap, respectively. The complex channel gain $h_i(t)$ can be described by the superposition of the LoS (line-of-sight) component $h_i^{LoS}(t)$ and the SB (single-bounced) component $h_i^{SB}(t)$ as in (2). The Rician factor and the mean power for the ith tap are denoted by K and Ω_i, respectively. The symbol $\tau(t) = \xi(t)/c$ is propagation time of the LoS path while $\tau_i(t) = (\xi_T(t) + \xi_R(t))/c$ stands for that of the SB path, where c is the velocity of light. The phase ψ_{n_i} is assumed to be uniform distributions over $[-\pi, \pi)$ and $f_{\max}$ is the maximum Doppler frequency.

TABLE I
DEFINITION OF PARAMETERS IN.

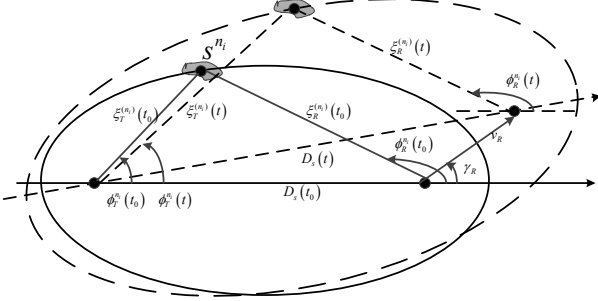| Parameters	Description
$\xi(t), \xi_T^i(t)$, and $\xi_R^i(t)$	Distances $d(BS, MRS), d(BS, s^{(n_i)})$, and $d(s^{(n_i)}, MRS)$, respectively
$d(s^{(n_i)}, MRS)$	MRS speed and the angle of motion, respectively
$\phi^{LoS}(t), \phi_R^{n_i}(t)$	AoA of the LoS path and AOA of the path trevelling form scatterer $s^{(n_i)}$ to the MSR

Fig. 2. The geometrical ellipse model for HST channels [20]

$$h_i(t) = h^{LoS}(t) + h^{SB}(t)$$

$$= \sqrt{\frac{K}{K+1}} e^{j-2\pi f_c \tau(t)} \times e^{j2\pi f_{\max} t \cos(\phi^{LoS}(t) - \gamma_R)} + \quad (2)$$

$$\sqrt{\frac{\Omega_i}{K+1}} \sum_{i=1}^{N_i} \frac{1}{\sqrt{N_1}} e^{j(\psi_{n_i} - 2\pi f_c \tau_{n_i}(t))} \times e^{j2\pi f_{\max} t \cos(\phi_R^{n_i}(t) - \gamma_R)}$$

The time-variant LoS AoA $\phi^{LoS}(t)$ is computed as
$\phi^{LoS}(t)$

$$= \begin{cases} \phi^{LoS}(t_0) + \arccos\left(\frac{D_s(t_0) + v_R t \cos\gamma_R}{D_s(t)}\right), & -\pi \le \gamma_R \le 0. \\ \\ \phi^{LoS}(t_0) - \arccos\left(\frac{D_s(t_0) + v_R t \cos\gamma_R}{D_s(t)}\right), & 0 \le \gamma_R \le \pi. \end{cases}$$
$$(3)$$

The distance between BS and MRS can be computed as

$$D_s(t) = \sqrt{D_s^2(t_0) + (v_R t)^2 + 2D_s(t_0) v_R t \cos\gamma_R}. \quad (4)$$

Using the geometrical relations and all the angles defined in Fig. 2, the mean angular value of the AoA $\mu_R^{(i)}$ is obtained as in (5). The AoA of SB path $\phi_R^{n_i}(t)$ can be described by the Mises probability density function (PDF)

$$f(\phi_R^i)(t) \triangleq \frac{\exp\left[k_R^{(i)} \cos\left(\phi_R^i - \mu_R^{(i)}(t)\right)\right]}{2\pi I_0\left(k_R^{(i)}\right)}, \quad (6)$$

where $k_R^{(i)}$ is the relevant von Mises parameter that controls the spread of ϕ_R^i.

Applying the modified method of equal areas (MMEA), the AoA of SB path $\{\phi_R^{n_i}(t)\}_{n_i=1}^{N_i}$ can be specified by solving the following equation

$$\frac{n_i - \frac{1}{4}}{N_i} - \int_{\mu_R^{(i)}(t_0)}^{\phi_R^{n_i}} f\left(\phi_R^i\right)(t_0) d\phi_R^i = 0, n_i = 1, 2, \ldots, N_i \quad (7)$$

Combining the results of $\{\phi_R^{n_i}(t)\}_{n_i=1}^{N_i}$ obtained in (7) and the power delay profile (PDP) of HST channel measurements, the parameters of the HST channel model can be derived [2].

III. INTERFERENCE ANALYSIS

In this section, the interference analysis of OFDM systems using the geometry-based HST channel model will be illustrated. The SINR of each sub-carrier at the HST-OFDM receiver has been computed. Using the result of SINRs, the capacity of the HST-OFDM has been derived. The Doppler effect that causes the ICI is assumed to be as a result the train movement. The frequency mismatch in the transmitter and the receiver oscillators is not considered here.

A. SINR Formulation

At the transmiter side, the baseband signal of an OFDM signal at the time t_n can be given by

$$x_n = \frac{1}{\sqrt{N}} \sum_{k=0}^{N-1} X_k \exp\left(\frac{j2\pi kn}{N}\right) \quad (8)$$

where X_k denotes the kth data-modulated subcarrier in the transmitted OFDM symbol and N is the number of subcarriers. After going through the time-variant HST channel, the received signal y_n is then obtained by

$$y_n = \frac{1}{\sqrt{N}} \sum_{n=0}^{N-1} H_{k,n} X_k e^{j2\pi nk/N} + w_n, \quad (9)$$

in which the w_n denotes the additive white Gaussian noise (AWGN); $H_{k,n}$ is the time-variant channel transfer function (TVCTF) of the HST channel which is obtained by taking

$$\mu_R^i(t) = \begin{cases} \gamma_R - \arccos\left(\frac{v_R t - \xi_R^{(n_i)}(t_0)\cos(\gamma_R - \mu_R^i(t_0))}{\sqrt{\xi_R^{2(n_i)}(t_0) + (v_R t)^2 - 2\xi_R^{(n_i)}(t_0) v_R t \cos(\gamma_R - \mu_R^i(t_0))}}\right), & -\pi \le \gamma_R \le 0. \\ \\ \gamma_R + \arccos\left(\frac{v_R t - \xi_R^{(n_i)}(t_0)\cos(\gamma_R - \mu_R^i(t_0))}{\sqrt{\xi_R^{2(n_i)}(t_0) + (v_R t)^2 - 2\xi_R^{(n_i)}(t_0) v_R t \cos(\gamma_R - \mu_R^i(t_0))}}\right), & 0 \le \gamma_R \le \pi. \end{cases} \quad (5)$$

the Fourier transform of the TVCIR $h(t_n, \tau)$ with respect to propagation delay τ.

After performing the FFT at the receiver side, the demodulated signal can be determined by

$$Y_k = S_k + I_k + W_k, \qquad (10)$$

where S_k, I_k, and W_k are the desired signal, the interference signal, and the AWGN in frequency domain, respectively. They can be computed as follows

$$S_k = \frac{1}{N} \sum_{n=0}^{N-1} H_{k,n} X_k \qquad (11)$$

and

$$I_k = \frac{1}{N} \sum_{\substack{m=0 \\ m \neq k}}^{N-1} \sum_{n=0}^{N-1} H_{m,n} X_m e^{j2\pi(m-k)n/N}. \qquad (12)$$

The SINR of the kth subcarrier at the OFDM receiver can be defined by

$$\text{SINR}_k = \frac{P_{D_k}}{P_{I_k} + P_{N_k}}, \qquad (13)$$

in which $P_{D_k} = P_{R_k} E\left[|S_k|^2\right]$, $P_{I_k} = P_{R_k} E\left[|I_k|^2\right]$, and $P_{N_k} = E\left[|W_k|^2\right]$ are the desired power, the interference power, and the noise power, respectively. The symbol P_{R_k} is the received power of kth subcarrier at the OFDM receiver.

Subsituting (11) and (12) into (13), the SINR_k can be given by

$$\text{SINR}_k = \frac{\left| \frac{1}{N} \sum_{n=0}^{N-1} H_{k,n} X_k \right|^2}{\left| \frac{1}{N} \sum_{\substack{m=0 \\ m \neq k}}^{N-1} \sum_{n=0}^{N-1} H_{m,n} X_m e^{j2\pi(m-k)n/N} \right|^2 + \frac{1}{\text{SNR}_k}}, \qquad (14)$$

where SNR_k stands for the signal-to-noise ratio of subcarrier at the OFDM receiver.

B. Capacity Analysis

The ergodic capacity of the kth subcarrier can be computed as

$$C_k = \Delta f \log_2(1 + \text{SINR}_k) \qquad (15)$$

in which the subcarrier spacing $\Delta f = B/N$, where B denotes the signal bandwidth.

Inter-symbol interference (ISI) can be avoided by selecting the guard length $T_G \geq \tau_{\max}$, where $\tau_{\max}$ is the maximal delay spread of the HST channel. Assuming each sub-carrier is loaded with data, the total channel capacity of the HST-OFDM system is obtained by [22]

$$C = \frac{T_S}{T_S + T_G} \Delta f \sum_{k=1}^{N-1} \log_2(1 + \text{SINR}_k), \qquad (16)$$

where T_S stands for the OFDM symbol duration. The ratio $\beta = T_S/(T_S + T_G)$ denotes the bandwidth efficiency of the

system. The capacity can also be expressed as C/B in bits per second per hertz (b/s/Hz)

$$\frac{C}{B} = \frac{T_S}{T_S + T_G} \times \frac{1}{N} \times \sum_{k=1}^{N-1} \log_2(1 + \text{SINR}_k) \qquad (17)$$

C. Constraints on Selecting HST-OFDM System Parameters

Based on the formulation of SINRs and capacity of the HST-OFDM system given in the previous subsection, a set of system parameters which are the bandwidth, the symbol duration, and the number of subcarriers should be considered thoughtfully to enhance spectral efficiency and also restrict the ICI effect. Assuming the guard length be chosen as a fixed value $T_G = \tau_{\max}$, where $\tau_{\max}$ is the maximum delay spread of the HST channel, observing (17), the constraints on selecting their system parameters should be analyzed as follows:

- *Symbol duration*: The capacity is on the increase if the larger symbol duration T_S is chosen. The reason for the increase on the capacity is that the larger symbol duration T_S results in the higher bandwidth efficiency β as shown in (17). On the other hand, the larger T_S causes the smaller subcarrier spacing $\Delta f = 1/T_S$ that makes the ICI effect be more severe. Consequently, the SINR is degraded because the increase of ICI power P_I as shown in (13). The SINR degradation will result in the capacity decrease as shown in (17.

- *Signal bandwidth and number of subcarriers*: For a specified symbol duration $T_S = N/B$, one can chose appropriate values of system bandwidth B and the number of subcarriers N. Available bandwidth for the system design is the scarce resource. Based on the bandwidth, the number of subcarriers will be determined. It is easily to fit in a large number of subcarriers with a large bandwidth. However, the large number of subcarriers causes the difficulty in implementing the synchronization unit at the receiver [6].

Because of these complex constrains, the parameters should be considered carefully when designing the HST-OFDM system. By analyzing the numerical results in the following section, they can be specified for each train speeds to meet the QoS requirements as long as reach the maximal capacity.

IV. NUMERICAL RESULTS

To configure the HST channel model, the HST channel measurement results in [21] have been used. The power delay profile (PDP) of the Close Area (CA) scenario, which has the maximum number of taps with the maximum delay spread $\tau_{\max} = 5.6\,\mu s$, is used to further investigated the HST-OFDM system. For the CA scenario, $D(t) \in (250\text{m}, 1550\text{m}]$, and the initial value is $D(t_o) = 800$m, the Rician factor $K = 5.9$. The PDP is used to computed the distance between different con-focal ellipses [2]. The initial AoA $\mu_R^{(i)}(t_0) = 45^o$ and the concentration parameter of the von Mise distribution $k_R^{(i)} = 6$ are chosen as in [23]. The movement angle of MSR speed is chosen as $\gamma_R = 30^0$. Table II illustrates the key parameters which were used to simulated the HST-OFDM system.

TABLE II
THE KEY PARAMETERS FOR SIMULATIONS.

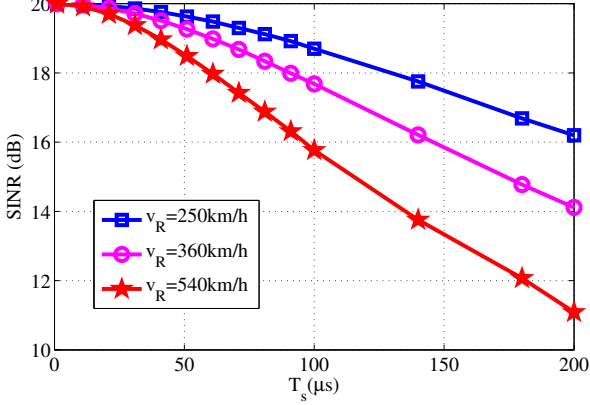| Parameters	Value
Carrier frequency (f_c)	2.6 GHz
Symbol duration (T_S)	$10\,\mu s - 200\,\mu s$
MSR moving speed (v_R)	250 km/h, 360 km/h, 540 km/h
Number of subcarriers (N)	512, 1024, 2048
Guard length ($T_G \geq \tau_{\max}$)	$5.6\mu s$

Fig. 3. SINR versus symbol duration for different train speeds with SNR = 20 dB

A. SINR results

To investigate SINR performance of HST-OFDM transmissions, Fig. 3 shows the SINR values versus the symbol duration T_S under different train speeds for the SNR of 20 dB. As observed, the SINR value decreases as the symbol duration increases. The SINR degradation is more severe for large symbol duration of $T_S > 50\mu s$. For a higher speed of train (i.e., the higher Doppler shifts), the large symbol duration can lead the SINR to degrade more quickly. The reason can be explained as the subcarrier spacing $\Delta f = 1/T_S$ will be narrower for a larger symbol duration T_S. That causes a stronger ICI effect and decreases the SINR. In contrast, for a smaller symbol duration of $T_S < 20\mu s$, the ICI effect can be neglect then the SINR values are almost same for different train speeds.

Moreover, the SINR results can be used as guidelines to specify the approriate symbol duration for the HST-OFDM system to meet a given QoS level (i.e., the SINR must be greater than a threshold value) for different HST movement scenarios. The SINR results shown in Fig. 4 are plotted for the train speed of $v_R = 540$ km/h. In particular, to achieve the required SINR of 20 dB and 25 dB, the OFDM symbol duration should be smaller than $75\mu s$ and $40\mu s$ for the SNR of 30 dB, respectively. However, for a fixed $T_G = 5.6\mu s$, the smaller T_S make the bandwidth efficiency β reduce that may result in degrading the system capacity as shown in (17). Therefore, in the next subsection 4.2, the capacity is evaluated
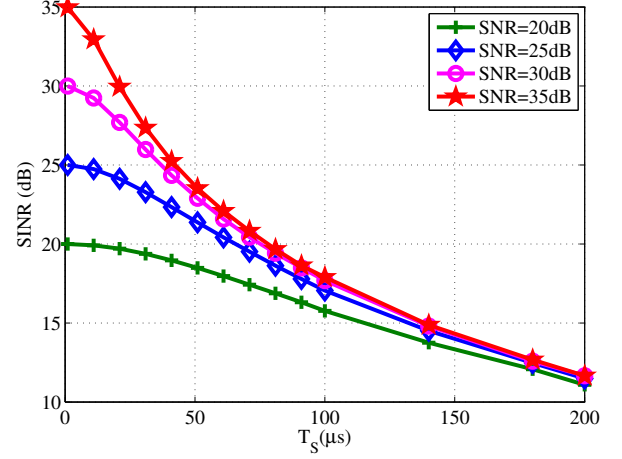

Fig. 4. SINR versus symbol duration for $v_R = 540$ km/h with different SNRs.
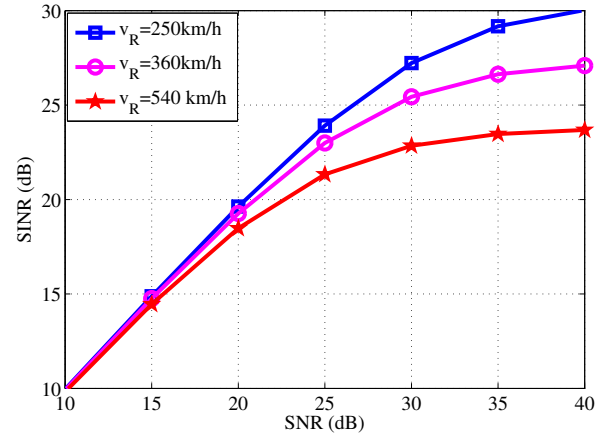

Fig. 5. SINR versus symbol duration for $v_R = 540$ km/h with different SNRs

in order to select the appropriate symbol duration that can maximize the capacity.

Furthermore, as shown in Fig. 4, it can be seen that for the symbol duration which is larger than $50\mu s$, with SNR of higher than 30 dB, the increase in SNR could not make the improvement in SINRs (i.e. the QoS). The cause of this phenomenon is that the higher SNR causes the mitigation of AWGN noise effect but the augment in ICI effect $P_{I_k} = P_{R_k}E\left[|I_k|^2\right]$. Consequently, the SINR computed in (13) could not been improved by increase SNR of higher than 30 dB. Figure 5 depicts the SINR versus SNR for different train speeds. Using these results, the highest SNR should be 30 dB and 35 dB for the train speeds of 540 km/h and 360 km/h. For the lower speed of 250 km/h, the ICI effect could be neglect for the SNR of lower than 25 dB. To summarize, the results plotted in Fig. 4 and Fig. 5 can be used to select the appropriate values of T_S and SNR (i.e. transmit power) to meet a given SINR threshold for different train speeds.
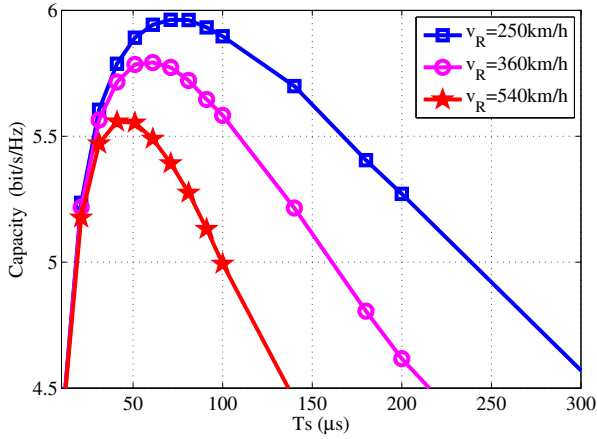
Fig. 6. Capacity versus T_S for different train speeds with SNR=20 dB

TABLE III
RESULTS OF THE HST-OFDM SYSTEM PARAMETERS FOR DIFFERENT
TRAIN SPEEDS WITH SNR=20 DB.

v_R	C	T_S	Bandwidth (MHz)		
(km/h)	(b/s/Hz)	(μs)	N=512	N=1024	N=2048
250	5.96	80	6.40	12.80	25.60
360	5.79	60	8.53	17.06	34.12
540	5.55	50	10.24	20.48	40.96

B. Capacity results

Figure 6 depicts the HST-OFDM capacity system versus symbol duration for different train speeds with SNR of 20 dB. As can be seen, one can choose the optimal symbol duration to achieve the maximal capacity for each train speeds. Namely, the optimal value T_S of $50\mu s$, $60\mu s$, and $80\mu s$ should be chosen for train speeds of $540\,\text{km/h}$, $360\,\text{km/h}$, and $250\,\text{km/h}$, respectively. Furthermore, using the results of optimal T_S, the appropriate bandwidths B and number of subcarriers N can be chosen for different cases of HST movement scenarios as shown in Table III. The high value of SNR can contribute to improve the capacity. However, the high SNR means the high transmit power that can be the reason for the increase of ICI power $P_{I_k} = P_{R_k} E \left[|I_k|^2 \right]$ where I_k is computed in (12). As a result, the HST-OFDM system could be more sensitive to the ICI effect.

To demonstrate the impact of SNR on the optimal value of T_S, the system capacity versus SNR for different SNRs with $v_R = 540\,\text{km/h}$, $v_R = 360\,\text{km/h}$, and $v_R = 250\,\text{km/h}$ are shown in Fig. 7, Fig. 8, and Fig. 9, respectively. It can be seen that the higher SNR is, the shorter optimal symbol duration T_S is to reach the maximal capacity. Because of the high SNR is responsible for the high sensitive ICI property of the HST-OFDM system, the symbol duration T_S should be chosen shorter to limit the ICI effect. The results of optimal HST-OFDM system parameters for different SNRs with train speeds of $v_R = 540\,\text{km/h}$, $360\,\text{km/h}$, and $250\,\text{km/h}$ are shown in Table. IV. Based on the hardware configuration of HST-
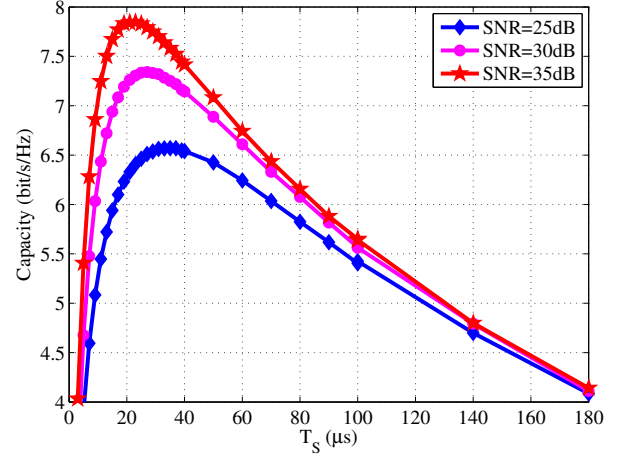
Fig. 7. Capacity versus T_S for $v_R = 540\,\text{km/h}$ with different SNRs.
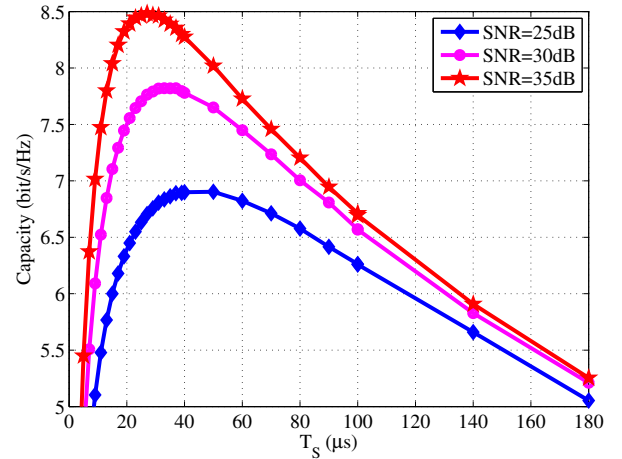
Fig. 8. Capacity versus T_S for $v_R = 360\,\text{km/h}$ with different SNRs
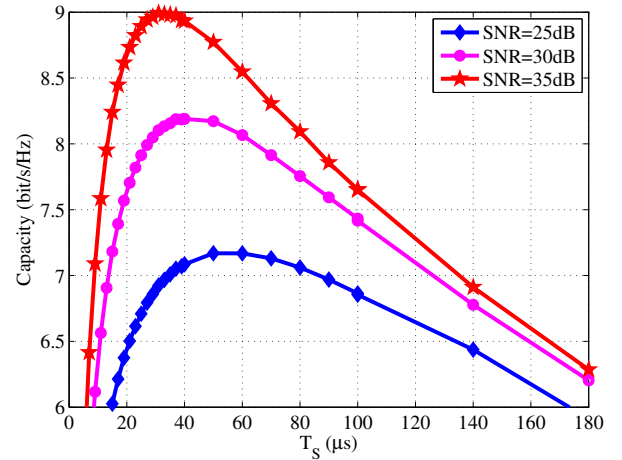
Fig. 9. Capacity versus T_S for $v_R = 250\,\text{km/h}$ with different SNRs

TABLE IV
RESULTS OF THE HST-OFDM SYSTEM PARAMETERS FOR DIFFERENT
TRAIN SPEEDS WITH DIFFERENT SNRs.

v_R (km/h)	SNR (dB)	T_S (μs)	C (b/s/Hz)	Bandwidth (MHz)		
				N=512	N=1024	N=2048
250	25	60	7.17	8.53	17.06	25.60
	30	40	8.19	12.80	25.60	51.20
	35	31	8.99	16.51	33.02	66.04
360	25	50	6.90	10.24	20.48	40.96
	30	37	7.82	13.84	27.68	55.36
	35	27	8.48	18.96	37.92	75.84
540	25	35	6.57	14.62	29.24	58.48
	30	27	7.34	18.96	37.92	75.84
	35	23	7.85	22.26	44.52	89.04

OFDM transceivers, the values of B and N should be selected to reach the maximal capacity.

V. CONCLUSION

This paper formulated SINR expression for HTS-OFDM transmissions using the non-stationary HST channel model. Consequently, the SINR is used as a figure of merit to evaluate the capacity and the HST- OFDM system performance. By analyzing the results of SINR and capacity, the appropriate OFDM transmission settings including the bandwidth, the symbol duration, and the number of subcarries can be chosen to satisfy a a given QoS requirement and to maximize the system capacity. These results can be used as theoretical guidelines in designing the HST-OFDM systems.

ACKNOWLEDGMENT

REFERENCES

[1] V. Vahidi and E. Saberinia, "OFDM high speed train communication systems in 5G cellular networks," in *2018 15th IEEE Annual Consumer Communications & Networking Conference (CCNC)*. IEEE, 2018, pp. 1–6.

[2] Y. Fu, C. Wang, A. Ghazal, e. M. Aggoune, and M. M. Alwakeel, "Performance investigation of spatial modulation systems under non-stationary wideband high-speed train channel models," *IEEE Transactions on Wireless Communications*, vol. 15, no. 9, pp. 6163–6174, 2016.

[3] V. Vahidi and E. Saberinia, "Channel estimation for wideband doubly selective UAS channels." Miami, FL, USA: IEEE, 2017, pp. 1175–1180.

[4] V. Vahidi, A. P. Yazdanpanah, E. Saberinia, and E. E. Regentova, "Channel estimation, equalisation, and evaluation for high-mobility airborne hyperspectral data transmission," *IET Communications*, vol. 10, pp. 2656–2662, 2016.

[5] A. Sanz-Gómara, J. A. Marín-García, and J. I. Alonso, "Performance evaluation of MIMO architectures with moving relays in high-speed railways," in *2018 48th European Microwave Conference (EuMC)*, 2018, pp. 716–719.

[6] M. N., R. M.I., K. S., and P. R., *OFDM: Principles and Challenges. In: Tarokh V. (eds) New Directions in Wireless Communications Research*. Springer, Boston, MA, 2009.

[7] J. Rodriguez-Pineiro, P. Suarez-Casal, M. Lerch, S. Caban, J. A. Garcia-Naya, L. Castedo, and M. Rupp, "LTE downlink performance in high speed trains." Glasgow: IEEE, 2015, pp. 1–5.

[8] Zhichao Sheng, Yong Fang, and Chen Wang, "A BEM method of channel estimation for OFDM systems in high-speed train environment," in *2013 International Workshop on High Mobility Wireless Communications (HMWC)*, 2013, pp. 6–9.

[9] B. Gong, L. Gui, Q. Qin, and X. Ren, "Compressive sensing-based detector design for SM-OFDM massive MIMO high speed train systems," *IEEE Transactions on Broadcasting*, vol. 63, no. 4, pp. 714–726, 2017.

[10] Z. Sheng, H. D. Tuan, and Y. Fang, "Power allocation for OFDM system in a high-speed train environment," in *2015 IEEE 26th Annual International Symposium on Personal, Indoor, and Mobile Radio Communications (PIMRC)*, 2015, pp. 650–655.

[11] X. Ren, M. Tao, and W. Chen, "Compressed channel estimation with position-based ICI elimination for high-mobility SIMO-OFDM systems," *IEEE Transactions on Vehicular Technology*, vol. 65, no. 8, pp. 6204–6216, 2016.

[12] Y. Xin, Z. Liang, Y. Bai, C. Zhai, and W. Li, "Capacity enhancement using cooperative distributed antenna system in downlink high-speed train environments," in *2019 11th International Conference on Wireless Communications and Signal Processing (WCSP)*, 2019, pp. 1–5.

[13] I. Zakia, "Capacity of HAP-MIMO channels for high-speed train communications," in *2017 3rd International Conference on Wireless and Telematics (ICWT)*, 2017, pp. 26–30.

[14] N. Lin, X. Huang, and X. Ma, "Analysis of the uplink capacity in the high-speed train wireless communication with full-duplex mobile relay," in *2016 IEEE 83rd Vehicular Technology Conference (VTC Spring)*, 2016, pp. 1–5.

[15] M. K. Bhatt, B. S. Sedani, K. R. Parmar, and M. P. Shah, "Ergodic UL/DL capacity analysis of co-located and distributed antenna configuration for high speed train with massive MIMO system," in *2017 International Conference on Inventive Computing and Informatics (ICICI)*, 2017, pp. 458–461.

[16] T. Zhou, C. Tao, L. Liu, J. Qiu, and R. Sun, "High-speed railway channel measurements and characterizations: a review," *Journal of Modern Transportation*, vol. 20, no. 4, pp. 199–205, 2012. [Online]. Available: https://doi.org/10.1007/BF03325799

[17] F. Kaltenberger, A. Byiringiro, G. Arvanitakis, R. Ghaddab, D. Nussbaum, R. Knopp, M. Bernineau, Y. Cocheril, H. Philippe, and E. Simon, "Broadband wireless channel measurements for high speed trains," in *2015 IEEE International Conference on Communications (ICC)*, 2015, pp. 2620–2625.

[18] Y. Bi, J. Zhang, Q. Zhu, W. Zhang, L. Tian, and P. Zhang, "A novel non-stationary high-speed train (HST) channel modeling and simulation method," *IEEE Transactions on Vehicular Technology*, vol. 68, no. 1, pp. 82–92, 2019.

[19] A. Ghazal, C. Wang, H. Haas, M. Beach, X. Lu, D. Yuan, and X. Ge, "A non-stationary MIMO channel model for high-speed train communication systems," in *2012 IEEE 75th Vehicular Technology Conference (VTC Spring)*, 2012, pp. 1–5.

[20] A. Ghazal, C. Wang, B. Ai, D. Yuan, and H. Haas, "A nonstationary wideband MIMO channel model for high-mobility intelligent transportation systems," *IEEE Transactions on Intelligent Transportation Systems*, vol. 16, no. 2, pp. 885–897, 2015.

[21] L. Liu, C. Tao, J. Qiu, H. Chen, L. Yu, W. Dong, and Y. Yuan, "Position-based modeling for wireless channel on high-speed railway under a viaduct at 2.35 GHz," *IEEE Journal on Selected Areas in Communications*, vol. 30, no. 4, pp. 834–845, 2012.

[22] Y. M. Aval, S. K. Wilson, and M. Stojanovic, "On the achievable rate of a class of acoustic channels and practical power allocation strategies for OFDM systems," *IEEE Journal of Oceanic Engineering*, vol. 40, no. 4, pp. 785–795, 2015.

[23] "Guidelines for evaluation of radio interface technologies for ITU," Geneva, Switzerland, Tech. Rep. Tech. Rep. ITU-R M.2135-1, 2009.